

Co-existence of Self-Organized Criticality and Intermittent Turbulence in an MHD Current Sheet with a Threshold Instability

Alexander J. Klimas,¹ Vadim M. Uritsky,^{2,*} and Maya Paczuski²

¹*NASA Goddard Space Flight Center, Greenbelt, MD 20771, USA*

²*Complexity Science Group, Department of Physics and Astronomy, University of Calgary, Calgary, Alberta, Canada T2N 1N4*

(Dated: May 26, 2019)

We report numerical evidence that self-organized criticality (SOC) and intermittent turbulence (IT) coexist in a current sheet model based on resistive magnetohydrodynamic (MHD) equations. The model also includes a local hysteretic switch to capture plasma physical processes outside of MHD, which are normally described as current-dependent resistivity. Results from numerical simulations show scale-free avalanches of magnetic energy dissipation characteristic of SOC, as well as multiscaling in the velocity field numerically indistinguishable from certain hierarchical turbulence theories. We argue that SOC and IT are complementary descriptions of dynamical states realized by driven current sheets – which occur ubiquitously in astrophysical and space plasmas.

PACS numbers: 05.40.-a, 52.35.Ra, 64.60.Ht

Most theoretical studies of self-organized criticality (SOC) [1, 2] – excepting e.g. [3] – focus on cellular models such as the BTW sandpile. On the other hand, many examples of SOC-like phenomena, such as avalanches with scale free statistics, occur in systems whose canonical descriptions invoke continuum equations such as the Navier-Stokes or magnetohydrodynamic (MHD) equations – appropriate to describe intermittent turbulence (IT). The proposal that SOC and IT could be distinguished by analyzing waiting times between bursts [4] turned out false [5]. Once a finite observation threshold (unavoidable in any physical measurement) is introduced, even the ordinary BTW sandpile exhibits scale free waiting time statistics similar to e.g. solar flares [5]. In fact, complementarity between SOC and IT has been argued to be realized in avalanching systems [5, 6, 7, 8, 9, 10, 11]. Simultaneous signatures of SOC and IT were found in the solar corona by analyzing a single, extended data set of high resolution images provided by SOHO [10]. Also, Earth’s magnetosphere produces power-law statistics of dissipative events [12, 13, 14] as well as intermittent plasma streams [15, 16]. Up to now, SOC has been proposed [17, 18] to occur in numerical fluid models but its potential complementarity with IT has not been clarified.

Here, we analyze a recently introduced model [17, 19] for a current sheet that supports a magnetic field reversal in an MHD plasma. Simultaneous signatures of SOC and IT are observed in its dynamics. The model contains measurable plasma parameters coupled through the full system of resistive MHD equations, with boundary conditions that allow a persistent current sheet to form. To describe local breakdown, where standard MHD equations fail and the true plasma equations must be invoked, we adapt the idea of E. Lu [20]: A current dependent threshold instability, taking the form of an hysteretic switch controlling plasma resistivity [17, 19], is used. With

a uniform drive, the model repeatedly undergoes large scale loading and unloading cycles. During the unloading cycles it exhibits hallmarks of SOC such as scale-free avalanches of magnetic energy transport leading to its dissipation in the reconnection zone. At the same time, fluctuations in the velocity field exhibit multiscaling consistent with hierarchical turbulence models [21, 22]. We argue that coexistence of SOC and IT is a robust property of continuum avalanching models, and predict it to be observed in many space and astrophysical plasmas.

Current sheets are a basic feature of MHD and have been a major focus in plasma physics [23, 24, 25]. Whenever an electric current is injected into a highly conductive fluid, magnetic forces tend to expel it from the fluid. As a result, most electric currents are compressed into relatively thin layers dividing plasmas into magnetic domains inside of which the currents are relatively weak. Current sheets, forming the boundaries of these domains, are thereby integral to the majority of long-lived structures observed in plasmas. In many cases, they also dominate plasma dynamics. Strong current sheets support reversed magnetic field configurations which are prone to collapse due to plasma instabilities arising near the regions of high current density [26, 27, 28]. This leads to magnetic reconnection, which may be the main mechanism of magnetic energy dissipation in astrophysical systems [23, 25, 29].

The 2d numerical model studied here was originally motivated by observations of Earth’s magnetotail, which is a driver for high-latitude geomagnetic activity [30]. The key plasma structure that controls geomagnetic substorms and is represented by our model is the large-scale cross-tail current sheet. The model consists of the full compressible, resistive MHD system, including a polytropic energy equation (see eq.(1) - (4) in [17] for a complete definition). In addition the local resistivity, D ,

obeys the following equations:

$$Q = \{ D_{min}, |J| < \beta J_c; D_{max}, |J| > J_c \} \quad (1)$$

$$\partial_t D = (Q(|J|) - D)/\tau, \quad (2)$$

which were adapted from Lu [20]. The function Q takes the value $D_{max} \approx 1$ wherever the local current density J exceeds a critical value J_c and returns to $D_{min} \ll D_{max}$ when the current density falls below βJ_c , with $\beta < 1$. Hence, the switch in Q is hysteretic. The transition from D_{min} to D_{max} represents the excitation and saturation of a kinetic current-driven instability over a time interval that is below the resolution of MHD and, hence, enters as an instantaneous transition. The transition from D_{max} to D_{min} represents the subsequent quenching of the instability. The resistivity, D , is assumed to grow or decay with a single time-scale τ that is slow compared to the simulation time step. The values of the model parameters used here can be found in [17].

We have obtained numerical solutions of the current sheet model on a 400×400 grid with $D_{min} \ll 1$ such that wherever $D = D_{min}$ the evolution is indistinguishable from ideal MHD over the observed time scales. A configuration of the model in a snapshot during an unloading phase is illustrated in Fig. 1. Plasma inflowing at the upper and lower boundaries carries magnetic flux with it, increasing the strength of the magnetic field reversal (and hence the electric currents in the current sheet). Eventually the current reaches $J = J_c$ somewhere – not necessarily at $z = 0$ – which starts an avalanche of magnetic flux transport toward the central region where flux is annihilated and converted to kinetic and thermal energy. This conversion process also drives plasma out of the region through the open boundary at the right. A small portion ($10^{-3} - 10^{-2}$) of the input magnetic energy is carried out through this boundary as well.

Eventually, the simulated plasma reaches a statistically stationary state in which the rates of magnetic energy and plasma mass flowing into the region are balanced, over long time scales, by the field annihilation rate and the outflow at the open boundary. After about 10^3 Alfvén traversal times, this state takes the form shown in Fig. 2 of *large scale global cycles* made of long laminar periods during which plasma is loaded into the system but no active grid sites (with $Q = D_{max}$) are generated, followed by highly erratic unloading periods during which the magnetic field undergoes local transitions between frozen and unfrozen states analogous to stick-slip behavior of SOC models [31, 32, 33]. As shown in Fig. 2, energy dissipation occurs only during the unloading phases. Equal time snapshots of the magnetic field configuration, velocity field and dissipating regions in the unloading regime are shown in Fig. 1. Although the magnetic field appears smooth, the corresponding velocity field for the plasma is highly intermittent while at the same time, well defined regions of intense dissipation appear.

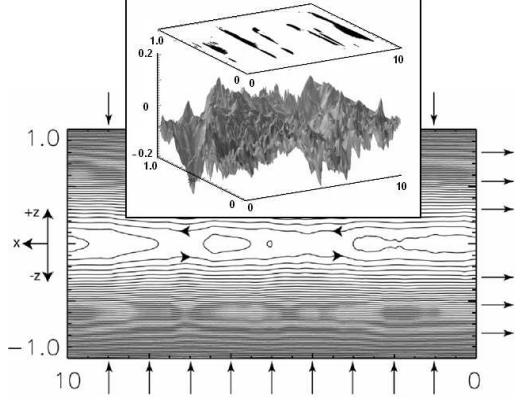


FIG. 1: Numerical simulation of a current sheet and its qualitative behavior (see [17] for details). The model is driven by a steady, uniform plasma inflow at the top and bottom boundaries as shown by arrows. The left boundary is closed, while the right is open. Plasma energized through annihilation in the magnetic field reversal leaves the region at the right. Inset: (Top) A snapshot of regions where the diffusive Poynting flux (see text) exceeds a threshold, used to define avalanches. (Bottom) At the same time, the corresponding velocity field (v_x) in the system. Note that while the magnetic field lines appear smooth at this scale, the plasma velocity field is highly intermittent.

Neglecting the convective contribution, the magnetic energy transported when a site becomes active is given by the magnitude $S_d(x, z) = (c/4\pi)\eta|\mathbf{J} \times \mathbf{B}|$ of the local diffusive Poynting flux [17], in which $\eta = 2\pi D/c^2$ is the anomalous resistivity, and c is the speed of light. To observe avalanches, we used an automated technique for detecting and tracing regions having grid sites with S_d above a certain threshold. In analogy with avalanches in 2d sandpiles, we treat the events as 2+1 dimensional spatiotemporal objects. Avalanches were identified by applying a floating activity threshold $S_{th}(t) = \langle S_d \rangle + k \cdot \sigma$ adjusted to the average value $\langle S_d \rangle$ and the standard deviation σ of the Poynting flux at every time step [39]. The time evolution of avalanches was obtained by checking the intersections of spatial regions above $S_{th}(t)$ in consecutive pairs of $S_d(x, z)$ snapshots. Each avalanche was characterized by its lifetime T and its total Poynting flux, E , obtained from the integration of S_d over its spatiotemporal domain – grid sites with $S_d(x, z, t) > S_{th}(t)$ taking part in the avalanche. The linear dimensions l_x and l_z of avalanches were estimated by determining standard deviations of the x and z coordinates over all the grid sites involved in each avalanche (equally weighted). In addition the geometric mean $l_{xz} \equiv (l_x l_z)^{1/2}$, as well as the total area s , representing the total number of distinct pixels involved in the avalanche, were estimated. The statistics reported here were obtained using $k = 3.0$ and have also been reproduced in the range $k = 1.5 - 4.0$.

The probability distribution for lengths, time, area, and energy of avalanches all obey scale free statistics. The first group of critical exponents was estimated based

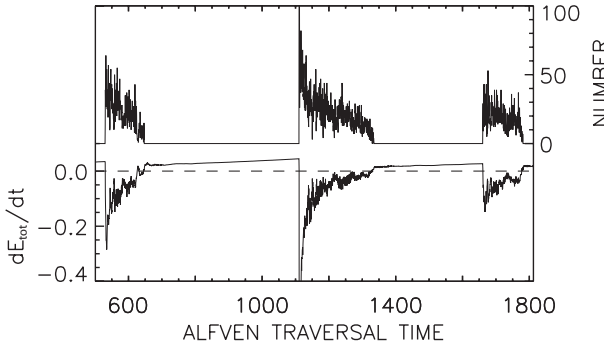


FIG. 2: Time series of the number of unstable grid sites with $Q = D_{max}$ through several cycles, and the corresponding time series of the total magnetic energy dissipation. Statistics shown in Figs. 3, 4 are obtained from the unloading cycles. Those separate quiet, laminar periods with no energy dissipation where the velocity field is smooth. Note that large scale loading and unloading do not occur for cellular automata models, such as the BTW sandpile, or for many models of IT – but do happen e.g. in magnetospheric dynamics [30].

on analyses of probability distributions $p(T, s_{max})$ and $p(E, s_{max})$ constructed from subsets with $s \leq s_{max}$, in which s_{max} is defined to be the maximum area (number of pixels) of events included in the subset used to make the histogram. The normalized probability distributions were studied using the scaling *ansatz*

$$p(X, s_{max}) = X^{-\tau_X} f_X(X/X_c), \quad X_c \sim s_{max}^{\lambda_X} \quad (3)$$

where $X \in \{E, T\}$ and f_X are scaling functions that are approximately constant for $X < X_c$ and drop rapidly for $X > X_c$. Assuming Eq. 3, we have plotted the distributions in the rescaled coordinates $(X/s_{max}^{\lambda_X}, p(X)X^{\tau_X})$ and identified the combination of τ_E , τ_T , λ_E and λ_T exponents that provides the best data collapse (Fig. 3). The resulting values $\tau_E = 1.48 \pm 0.02$ and $\tau_T = 1.95 \pm 0.03$ coincide with those reported earlier in [17]. The exponents $\lambda_E = 1.47 \pm 0.03$ and $\lambda_T = 0.68 \pm 0.04$ are consistent with the regression analyses for the expected values of energy and lifetime for avalanches with a given size s $\langle E \rangle_s$ and $\langle T \rangle_s$, within statistical error. These values also preserve the scaling relation $\lambda_T(\tau_T - 1) = \lambda_E(\tau_E - 1)$.

The anisotropy of the model leads to different growth rates of avalanches in the x and z directions. Hence $\langle s \rangle_{l_x} \sim (l_x)^{d_x}$ and $\langle s \rangle_{l_z} \sim (l_z)^{d_z}$ with $d_x = 1.40 \pm 0.03$ and $d_z = 3.11 \pm 0.06$. The geometric mean l_{xz} is related to s through another scaling relation, $\langle s \rangle_{l_{xz}} \sim (l_{xz})^{d_{xz}}$, with $d_{xz} = 1.97 \pm 0.05$ indicating that avalanches are compact. The exponent values obtained are consistent with $d_x^{-1} + d_z^{-1} = 2d_{xz}^{-1}$. We also studied E and T as functions of l_x and l_z and found that $\langle E \rangle_{l_x} \sim l_x^{\mu_x}$, $\langle T \rangle_{l_x} \sim l_x^{\nu_x}$, $\langle E \rangle_{l_z} \sim l_z^{\mu_z}$ and $\langle T \rangle_{l_z} \sim l_z^{\nu_z}$ with scaling exponents $\mu_x = 1.87 \pm 0.04$, $\nu_x = 1.13 \pm 0.01$, $\mu_z = 3.50 \pm 0.04$ and $\nu_z = 1.97 \pm 0.06$ (see the insets in Fig. 3). The ratios μ_x/μ_z and ν_x/ν_z are close to d_x/d_z as expected.

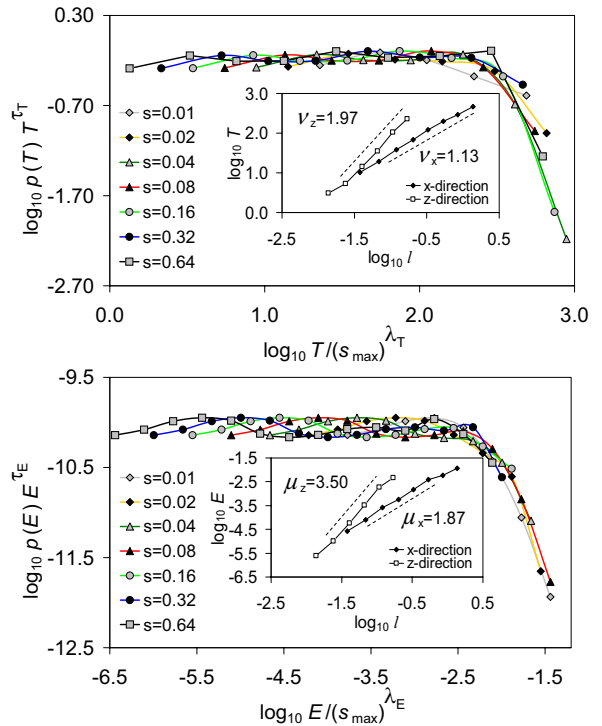


FIG. 3: Data collapse using Eq. 3 for avalanches with different maximum area s_{max} with $\tau_T = 1.95$, $\lambda_T = 0.68$, $\tau_E = 1.48$, and $\lambda_E = 1.47$. Insets: anisotropic scaling of E and T with the maximum avalanche extent l in x and z directions.

All these results indicate that with respect to bursts of energy dissipation above background, the system operates in at or near a SOC state.

To analyze the velocity field, we have followed the usual procedure by computing a set of equal time structure functions defined as $S_q(l) = \langle |\delta v_l|^q \rangle$, where $\delta v_l = (\mathbf{v}(\mathbf{r} + \mathbf{l}) - \mathbf{v}(\mathbf{r})) \cdot \mathbf{l}/l$ is the increment of the velocity \mathbf{v} in the direction \mathbf{l} (parallel to x or z axes), q is the order of the structure function, $l \equiv |\mathbf{l}|$ is the spatial displacement, and averaging indicated by $\langle \dots \rangle$ is performed over all positions \mathbf{r} and times during an unloading phase. For turbulent phenomena, within the inertial range, $S_q(l) \sim l^{\zeta(q)}$ with $\zeta(q)$ defined by the turbulent regime under study. To extend the range and improve the accuracy of this analysis, we have applied the method of extended self similarity (ESS) [34] by plotting $S_q(l)$ versus $S_3(l)$.

The resulting structure functions (Fig. 4) exhibit ESS over the entire range of scales available. The error bars shown are for $\zeta(q)/\zeta(3)$ in x direction; the errors in the z direction are about three times smaller. The values obtained in both directions are the same up to these errors. The dependence of $\zeta(q)/\zeta(3)$ on the order q shows a systematic departure from the Kolmogorov law $\zeta = q/3$. It can be accurately described by the hierarchical model $\zeta(q) = (1 - \gamma)q/g + C(1 - [1 - \gamma/C]^{q/g})$, in which C is the codimension of the most singular dissipative structures, g and γ are defined by $\delta z \sim \ell^{1/g}$ and $t_e \sim \ell^{\gamma}$, with

t_e being the energy transfer time at the smallest inertial scales ℓ [35]. We applied three sets of parameters corresponding to the original model of hydrodynamic turbulence due to She and Leveque (SL) [21] ($g = 3, \gamma = 2/3, C = 2$) as well as its extensions to MHD based on the Iroshnikov-Kraichnan theory (IK) [22] ($g = 4, \gamma = 1/2, C = 1$) and the Müller and Biskamp (MB) [36] theory ($g = 3, \gamma = 2/3, C = 1$). Both SL and IK provide reasonable fits to our data – where they are almost indistinguishable [40]. Fig. 4 also shows simulations results for 2d MHD turbulence [37] – confirming that the mechanism of intermittency in our avalanching MHD model can be empirically distinguished from the usual MHD, or, in other words, that avalanche mechanisms outside of MHD must be included to describe plasma processes where those mechanisms occur.

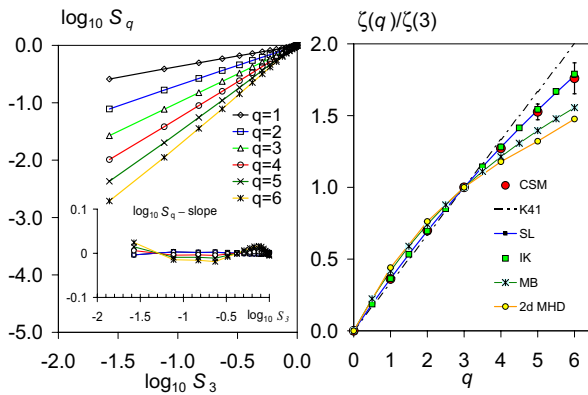


FIG. 4: Left: ESS plots of velocity structure functions with l parallel to z axis. The inset shows the same functions with subtracted average slopes. Right: Dependence of $\zeta(q)/\zeta(3)$ on the order q for our current sheet model (CSM), hierarchical models of IT, Kolmogorov model (K41) [38], as well as the exponents from 2d MHD simulations [37].

Our results indicate that coexistence of SOC and IT may be a generic property of driven current sheets – which are ubiquitous in nature. We studied an MHD model that includes a hysteretic, current driven instability for the magnetic resistivity. It exhibits power law avalanche statistics over a wide range of scales. These are described by critical exponents that satisfy expected scaling relations for SOC, and are stable under significant changes of model parameters and the avalanche detection threshold. At the same time, structure functions in the velocity field measured using ESS exhibit scaling behavior that agrees with hierarchical models of turbulence, but disagrees with results from other 2d MHD simulations that do not include effects of plasma instabilities outside of MHD. Our numerical results reinforce the prior observation of coexisting signatures of SOC and IT in a single data set of ultraviolet images of solar corona [10], and their robust co-appearance suggests that they are complementary phenomena expected to be simultane-

ously measurable in many astrophysical systems.

The work of A. J. K. was supported by the NASA Geospace Sciences program.

* Also at the Institute of Physics, Saint Petersburg University, Russia

- [1] P. Bak et al., Phys. Rev. Lett. **59**, 381 (1987).
- [2] P. Bak et al., Phys. Rev. A **38**, 364 (1988).
- [3] D. Hughes et al., Phys. Rev. Lett. **90**, 131101 (2003).
- [4] G. Boffetta et al., Phys. Rev. Lett. **83**, 4662 (1999).
- [5] M. Paczuski et al., Phys. Rev. Lett. **95**, 181102 (2005).
- [6] P. Bak and M. Paczuski, Physica A **348**, 277 (2005).
- [7] K. Chen et al., Physica A **340**, 566 (2003).
- [8] K. Chen and C. Jayaprakash, Physica A **340**, 566 (2004).
- [9] K. R. Sreenivasan et al., Physica A **340**, 574 (2004).
- [10] V. M. Uritsky et al., e-print **astro-ph/0610130** (2006).
- [11] T. Chang, Phys. Plasmas **6**, 4137 (1999).
- [12] V. M. Uritsky et al., J. Geophys. Res.–Space Physics **107**, 1426 (2002).
- [13] V. M. Uritsky et al., Geophys. Res. Lett. **30**, 1813 (2003).
- [14] V. M. Uritsky et al., Geophys. Res. Lett. **33**, L08102 (2006).
- [15] A. T. Y. Lui et al., Annales Geophysicae **24**, 2005 (2006).
- [16] Z. Voros et al., Space Sci. Rev. **122**, 301 (2006).
- [17] A. J. Klimas et al., J. Geophys. Res.–Space Physics **109**, 1426 (2004).
- [18] P. Dmitruk and D. O. Gomez, Astrophys. J. **484**, L83 (1997).
- [19] A. J. Klimas et al., Geophys. Res. Lett. **32**, L14108 (2005).
- [20] E. T. Lu, Phys. Rev. Lett. **74**, 2511 (1995).
- [21] Z.-S. She and E. Leveque, Phys. Rev. Lett. **72**, 336 (1994).
- [22] R. Grauer et al., Phys. Lett. A **195**, 335 (1994).
- [23] E. R. Priest and T. G. Forbes, *Magnetic Reconnection: MHD Theory and Applications* (Cambridge Univ. Press, 2000).
- [24] M. J. Aschwanden, *Physics of the Solar Corona* (Springer, 2005).
- [25] S. W. H. Cowley et al., Philos. Trans. Royal Soc. London A **361**, 113 (2003).
- [26] N. F. Loureiro et al., Phys. Rev. Lett. **95**, 235003 (2005).
- [27] A. T. Y. Lui, J. Geophys. Res.–Space Physics **101**, 13067 (1996).
- [28] S. W. H. Cowley et al., Phys. Reports **283**, 227 (1997).
- [29] V. S. Semenov et al., Planet. Space Sci. **40**, 63 (1992).
- [30] D. N. Baker et al., J. Geophys. Res.–Space Physics **104**, 14601 (1999).
- [31] P. Bak and C. Tang, J. Geoph. Res.–Solid Earth and Planets **94**, 15635 (1989).
- [32] Z. Olami et al., Phys. Rev. Lett. **68**, 1244 (1992).
- [33] M. Paczuski et al., Phys. Rev. E **53**, 414 (1996).
- [34] R. Benzi et al., Phys. Rev. E **48**, R29 (1993).
- [35] H. Politano and A. Pouquet, Phys. Rev. E **52**, 636 (1995).
- [36] W.-C. Müller and D. Biskamp, Phys. Rev. Lett. **84**, 475 (2000).
- [37] H. Politano et al., Europhys. Lett. **43**, 516 (1998).
- [38] A. Kolmogorov, Dokl. Akad. Nauk SSSR **31**, 538 (1941).
- [39] The floating threshold allows improved statistics considering the time variation during unloading cycles

[40] More direct information on the geometry of dissipative structures can be obtained from a 3d version of this

model, which will be described in a separate paper.